Oil Shale, 2021, Vol. 38, No. 3, pp. 181–198
doi: https://doi.org/10.3176/oil.2021.3.01

Structural characterization of Huadian oil shale kerogen by using ^{13}C DP/MAS NMR

Xiaoye Wang[(a)], Yulong You[(a)], Mao Mu[(a)], Xiangxin Han[(a)], Jie Shu[(b)*], Xiumin Jiang[(a)*]

[(a)] School of Mechanical Engineering, Shanghai Jiao Tong University, Shanghai 200240, China
[(b)] Analysis and Testing Center, Soochow University, Suzhou 215123, China

Received 5.11.2020, accepted 23.07.2021, available online 10.09.2021

Abstract. *Quantitative ^{13}C direct polarization/magic angle spinning (DP/MAS) solid-state nuclear magnetic resonance (SSNMR) was used to characterize type I kerogen isolated from Huadian oil shale. The DP/MAS results showed that this kerogen was highly aliphatic and its aromaticity (f_a) was as low as 20.23%. The average aliphatic carbon chain length (Cn), average aromatic cluster size (C) and substitute degree of aromatic rings (σ) were calculated. The NMR-derived H/C and O/C atomic ratios ($R_{H/C}$ and $R_{O/C}$) obtained by DP were in agreement with the corresponding results of ultimate analysis, indicating the accuracy of DP for quantification. Besides, using varying contact times cross polarization (CP) spectra were obtained at the same MAS frequency as the DP spectrum. Regardless of contact time, the aromaticities derived from CP were much lower than that from DP. Consequently, the $R_{H/C}$ value from CP was significantly higher than that of ultimate analysis. The contribution of spinning sidebands could be ignored with the MAS frequency up to 10 kHz. It is concluded that DP with a high MAS frequency is necessary for gaining quantitative structural information about kerogen, especially for its molecular modeling.*

Keywords: *type I kerogen, molecular structure, solid-state nuclear magnetic resonance, quantification, direct polarization.*

1. Introduction

Oil shale is a sedimentary rock containing organic matter finely disseminated in the mineral matrix of the shale, and the organic matter exists mainly in the form of kerogen, from which shale oil, a substitute for conventional crude oil,

* Corresponding authors: e-mails *shujie@suda.edu.cn, xiuminjiang@sjtu.edu.cn*

© 2021 Authors. This is an Open Access article distributed under the terms and conditions of the Creative Commons Attribution-NonCommercial 4.0 International License (http://creativecommons.org/licenses/by-nc/4.0/).

can be produced upon pyrolysis [1]. The chemical structure of kerogen not only has a fundamental influence on the yield, properties and composition of shale oil, but also determines some subproblems such as semi-coke properties [2] and pollutant emission [3]. Unfortunately, kerogen is an extremely complex mixture of macromolecules [4] and is insoluble in common organic solvents [1], making it very difficult to obtain information about its microstructure. In view of this, many techniques, such as solid-state nuclear magnetic resonance (SSNMR), X-ray photoelectron spectroscopy (XPS), Fourier transform infrared (FTIR), etc., have been applied to the characterization of kerogen [5–11].

^{13}C SSNMR spectroscopy is one of the most powerful techniques that has been used to study kerogen [12]. The most popular technique employed for carrying out ^{13}C SSNMR studies is cross polarization (CP), which enhances the ^{13}C NMR sensitivity and reduces the measuring time via transferring polarization from abundant ^{1}H spins to dilute ^{13}C spins [13]. In combination with the magic angle spinning (MAS) technique, which removes the line broadening caused by chemical shift anisotropy (CSA) and inter-nuclear dipolar coupling, the recorded CP/MAS spectra mostly demonstrate improved resolution with enhanced sensitivity. With the advantages of wide chemical shift range and according to the information on the ^{13}C chemical shifts-based fingerprints of functional groups, ^{13}C CP/MAS NMR is especially suitable for the structural characterization of complex organic matter like kerogen [5, 8, 14–16].

Recently, based on the data of ^{13}C CP/MAS NMR, several works have been conducted using molecular dynamic or quantum chemical calculations [17–21] to build three-dimensional macromolecular models of kerogens and to analyze the relevant reaction mechanism. In theory, such studies require highly accurate experimental data because of the sensitivity of simulation results to the structural parameters of the models [19, 20, 22]. However, the quantification of CP/MAS for kerogen has been a controversial issue for a long time [23–28]. The major problem is that all the acquired carbon signals in CP/MAS spectra demonstrate unequal ^{1}H→^{13}C CP enhancement factors. The non-protonated carbons and mobile components commonly present reduced CP efficiencies. As a consequence, the fraction of aromatic carbons can be greatly underestimated by CP [24, 25, 29]. Besides, another essential factor that makes CP/MAS spectra non-quantitative for kerogen is spinning sidebands. When the MAS frequency is markedly lower than the CSA of a specific carbon unit, the spinning sidebands show up in the spectra, reducing the intensity of the centerband and overlapping with the other carbon resonances. Therefore, CP/MAS spectra are not quantitative and are applicable only for qualitative and semiquantitative analyses.

Direct polarization/magic angle spinning (DP/MAS) at a sufficiently high spinning frequency is a quantitatively reliable technique, in which direct polarization (DP), also known as single pulse excitation (SPE) or Bloch decay (BD), is used to excite carbon nuclei directly with a 90° radiofrequency

pulse rather than magnetization transfer from ^{1}H spins and to show signals of all carbon types in true proportions. In addition, fast MAS can remove the influence of spinning sidebands. Despite the advantage of quantification, only a few ^{13}C DP/MAS NMR studies on kerogen have been published [27, 30–32] because DP/MAS experiments are much more time-consuming than CP/MAS experiments. Fortunately, the ^{13}C spin-lattice relaxation time ($T_{1,C}$) for most natural organic matter samples is not very long [33, 34]. Generally, a quantitative DP/MAS spectrum with a reasonable signal to noise ratio can usually be obtained within 15 h [28], which is acceptable when accurate structural parameters of kerogen are needed.

In this study, ^{13}C DP/MAS NMR at a sufficiently high spinning frequency is used for gaining accurate structural information on type I kerogen isolated from Huadian oil shale. In addition, CP spectra using three different contact times are also recorded. The structural parameters derived from CP are compared with those from DP in parallel. The results show that DP is reliable and necessary for a quantitative characterization and molecular modeling of kerogen.

2. Experimental section

2.1. Kerogen sample description

The kerogen analyzed in this study originates from the oil shale sample taken from Dachengzi mine located in Huadian city, China. In order to isolate kerogen, the shale sample was crushed and sieved to a size range of 0–0.25 mm, and then demineralized with HCl/HF by the standard procedure described by Durand and Nicaise [35]. The results of ultimate analysis of kerogen are given in Table 1. The kerogen purity was determined to be 96.8% by summing up the contents of the fractions of carbon, hydrogen, oxygen, nitrogen and sulfur (CHONS). According to the H/C vs O/C atomic ratio, Huadian oil shale kerogen belongs to type I, which suggests its high aliphaticity and low aromatic structures content [1].

Table 1. Ultimate analysis of Huadian oil shale kerogen, wt%, dry ash free basis

C	72.17
H	9.48
O[a]	11.77
N	1.38
S[b]	1.98
H/C[c]	1.576
O/C[c]	0.122

[a] organic oxygen, [b] total sulfur, [c] atomic ratio

2.2. SSNMR experimental conditions

Solid-state nuclear magnetic resonance experiments were performed on a Bruker AVANCE III HD 400 spectrometer operating at a Larmor frequency of 100.64 MHz for ^{13}C. The instrument was equipped with an H/X double-resonance magic-angle spinning probe, supporting the MAS rotor having a 4 mm outer diameter. The MAS frequency for all the experiments was 10 kHz. The quantitative ^{13}C DP/MAS NMR experiment was performed using a 4.6-μs (90°) ^{13}C pulse corresponding to 54.3 kHz rf frequency. The spectra were accumulated with 4096 scans. The recycle delay was 50 s, which was determined to ensure that all the ^{13}C nuclei were fully relaxed. ^{13}C CP/MAS NMR spectra were acquired using three different contact times: 0.5, 1 and 2 ms. The rf frequency for the ^{1}H 90° pulse was 62.5 kHz, corresponding to the pulse length of 4 μs. 3072 scans were collected for each CP/MAS spectrum, with a 3-s recycle delay between the scans. The sweep width for both CP and DP spectra was 40 kHz and each free induction decay (FID) contained 1218 data points, corresponding to the acquisition time of 15 ms. After data acquisition, all the FIDs were zero-filled to 32768 data points and processed using a Lorentz-to-Gaussian window function with a Lorentzian line broadening of 1 Hz and a Gaussian maximum position of 0.01. The ^{13}C chemical shifts were referenced with respect to tetramethyl silane (TMS) using solid adamantane (^{13}C, 29.46 ppm) as a secondary reference.

The decomposition and fitting of ^{13}C NMR spectra were performed using the DMFIT program [36] to determine the relative proportion of different carbon types. Gaussian/Lorentzian lines were used for fitting. The intensities, widths at half-maximum and Gaussian/Lorentzian ratios were optimized to give the best fit to the experimental spectra. The relative content of each carbon unit was calculated by the peak areas, which were given automatically by the program.

3. Results and discussion

3.1. Band assignments in a quantitative ^{13}C DP/MAS NMR spectrum

A quantitative ^{13}C DP/MAS NMR spectrum is shown in Figure 1a. The spectrum displays the features of type I kerogen, with a strong narrow band at ca 30 ppm and a weak broad band at ca 130 ppm, corresponding to sp^3- and sp^2-hybridized carbons, respectively, which is consistent with previous studies [16, 37]. With reference to relevant literature [5, 15, 16], seven aliphatic carbon types and six aromatic units were identified. The assignments of carbon resonances are summarized in Table 2. Remarkably, two weak bands at 25.5 ppm and 33.2 ppm covered by the main methylene band (30.6 ppm) were also assigned to methylene carbon, considering that part of the methylene carbon was affected by substituent electronegativity or γ-gauche effect. Likewise, the bands at 39.3 ppm and 43.9 ppm were assigned to methine carbon.

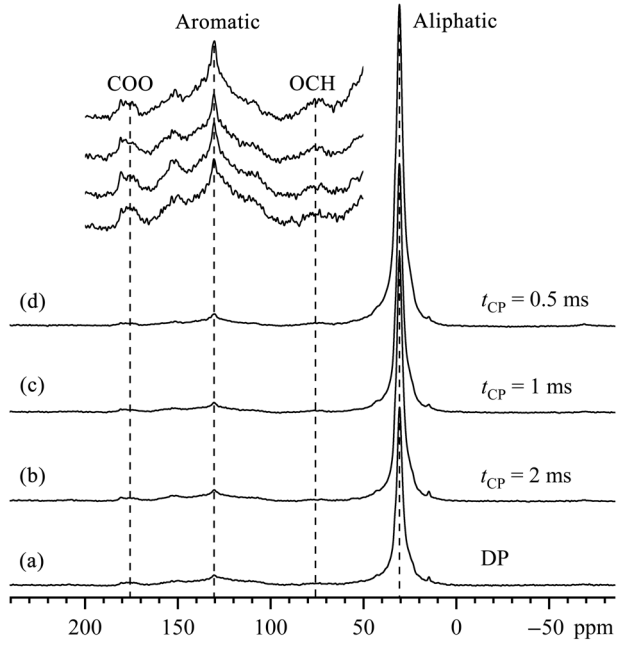

Fig. 1. Solid-state ^{13}C NMR spectra of Huadian oil shale kerogen obtained by DP (a) and CP using contact times (t_{CP}) of 2 ms (b), 1 ms (c) and 0.5 ms (d). The spectra are scaled to an identical intensity of the main aromatic peak for a quantitative comparison between CP and DP spectra.

Quaternary aliphatic carbon and C = C groups have been introduced into several previously proposed kerogen models [19, 38, 39]. However, the fast pyrolysis study of Huadian oil shale by Huang et al. [40] shows that no adamantane-like structures exist in the pyrolysis products and almost all alkenes generated are α-alkenes, indicating that the content of quaternary aliphatic carbon and C = C groups in the kerogen is negligible. Thus, no carbon resonance was assigned to them.

Besides, carbon units of O–C–O, such as anomeric, methylenedioxy, etc., were excluded from band assignments since O–C–O groups are generally not present in kerogen, except for the extremely immature kerogen with an exceptionally high O/C atomic ratio, ca 0.30 [14, 31]. Considering this, it is reasonable to assume that at most one oxygen atom is bound to the same carbon atom by a single bond, e.g., methoxy, alcohol, phenolic, in this kerogen.

Table 2. Assignments and relative areas of bands in a quantitative ^{13}C DP/MAS NMR spectrum

Carbon type	Character	Location	Chemical shift, ppm	Relative area, %	Fraction in model, %
Aliphatic methyl	f_{al}^{1}	—CH3	14.7	0.74	0.84
Aromatic methyl	f_{al}^{a}	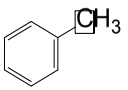	19.7	0.14	0.42
Aliphatic C2	f_{al}^{2t}	—CH2—CH2—CH3	23.4	0.32	0.84
Methylene	f_{al}^{2}	—CH2—CH2—CH2—	25.5 30.6 33.2	66.79	63.9
Methine	f_{al}^{3}	—CH	39.3 43.9	4.34	4.40
Oxy-methylene	f_{al}^{O2}	—CH2—O—	51.4	2.34	4.40
Oxy-methine	f_{al}^{O3}	HC—O—	76.1	2.69	2.30
Ortho-oxy-aromatic protonated	f_{a}^{HO}	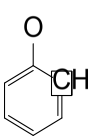	109.4	3.80	3.77

Table 2 (continued)

Carbon type	Character	Location	Chemical shift, ppm	Relative area, %	Fraction in model, %
Ortho-oxy-aromatic branched	f_a^{SO}	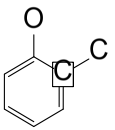	119.0	2.11	2.52
Aromatic protonated	f_a^{H}		126.1	3.14	2.94
Bridging ring junction	f_a^{B}	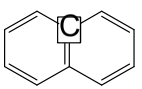	130.7	2.98	2.51
Aromatic branched	f_a^{S}	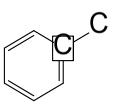	138.1	4.29	4.40
Oxy-aromatic	f_a^{O}	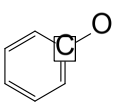	152.1	3.91	3.98
Carboxyl	f_{COO}		176.2	1.72	2.10
Carbonyl	f_{CO}		200–220	0.69	0.63

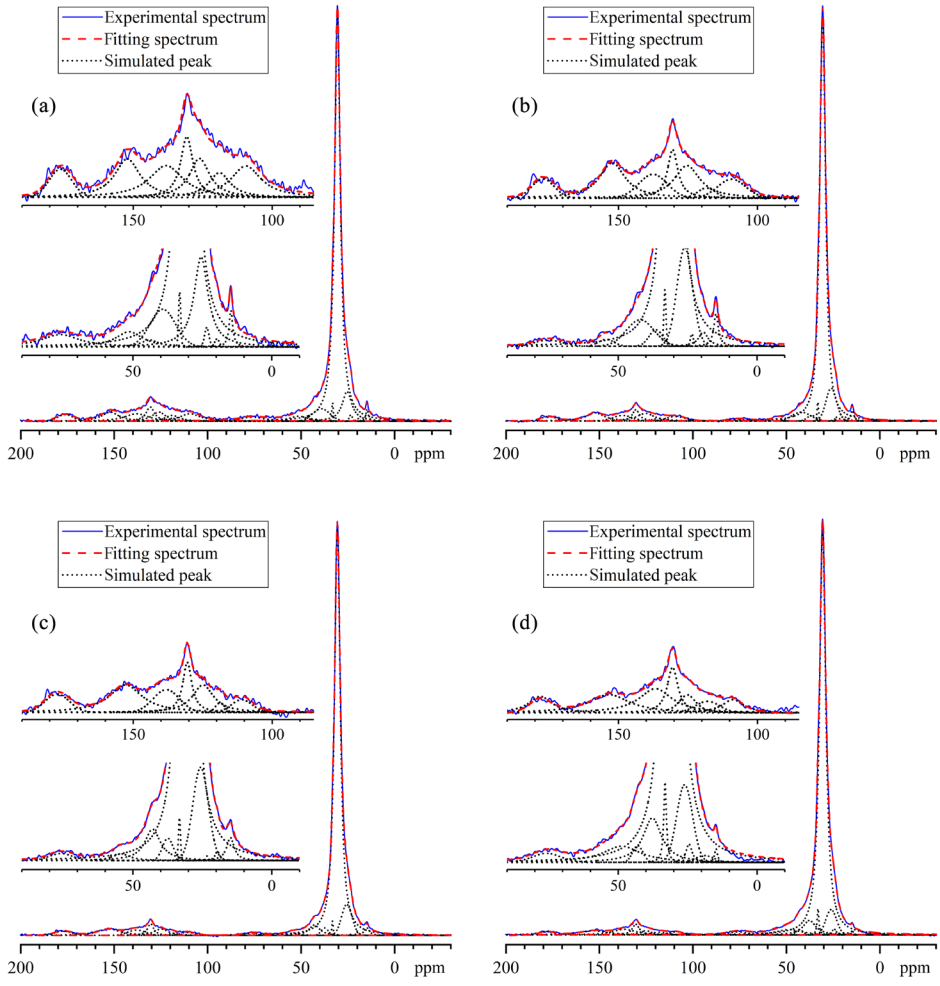

Fig. 2. The fitting spectrum and simulated peaks of ^{13}C DP/MAS NMR spectrum (a) and ^{13}C CP/MAS NMR spectra using contact times of 2 ms (b), 1 ms (c) and 0.5 ms (d).

3.2. Fractions of carbon units

Since the DP spectrum exhibits all carbon signals in the correct proportions, the relative areas of carbon bands, i.e. the ratios of the integrated band intensities to the integrated intensity of the entire spectrum, are equal to those of the fractions of carbon units. Spectral decomposition and fitting were performed to determine the area of each carbon type because of the band overlapping. The simulated peaks were arranged according to the carbon resonance assignments (Fig. 2a). As the three resonances in the regions of 0–90 ppm

(aliphatic carbons), 90–200 ppm (aromatic and carboxyl carbons) and 200–220 ppm (carbonyl carbon) did not overlap with each other, an accurate area of each band group was obtained by integration. The fitting of the DP spectrum was performed separately in the first two regions for a rapid convergence of iterations. The fitting spectrum reproduces the features of the experimental spectrum satisfactorily, as shown in Figure 2a. The widths of all the simulated peaks are within a reasonable range. The normalized areas of the simulated peaks are given in Table 2.

3.3. Structural parameters of kerogen

Compared with the fractions of carbon types, structural parameters can better describe the features of kerogen structure [8, 41]. The structural parameters used in this work are listed in Table 3 along with their definitions. The parameters were calculated using the carbon type fractions derived from the DP spectrum. The values of the structural parameters are presented in Table 4. As expected, the kerogen structure is dominated by aliphatic carbon units, and its aromaticity (f_a) is only 20.23%.

Table 3. Definitions of structural parameters of kerogen

Structural parameter	Character	Definition
Aromaticity	f_a	$f_a = f_a^{HO} + f_a^{SO} + f_a^{H} + f_a^{B} + f_a^{S} + f_a^{O}$
Aliphaticity	f_{al}	$f_{al} = f_{al}^{1} + f_{al}^{a} + f_{al}^{2t} + f_{al}^{2} + f_{al}^{3} + f_{al}^{O2} + f_{al}^{O3}$
Average aliphatic carbon chain length	Cn	$f_{al}/\left(f_a^{SO} + f_a^{S} + f_a^{O}\right) \le Cn \le f_{al}/\left(f_a^{SO} + f_a^{S}\right)$
Substitute degree of aromatic rings	σ	$\sigma = \left(f_a^{SO} + f_a^{S} + f_a^{O}\right)/f_a$
Average carbons per aromatic cluster	C	$C = 6f_a/\left(f_a - 2f_a^{B}\right)$
H/C atomic ratio from NMR	$R_{H/C}$	$R_{H/C} = 3\left(f_{al}^{1} + f_{al}^{a}\right) + 2\left(f_{al}^{2t} + f_{al}^{2} + f_{al}^{O2}\right) + f_{al}^{3} + f_{al}^{O3} + f_a^{HO} + f_a^{H} + f_{COO}$
O/C atomic ratio from NMR	$R_{O/C}$	$\left(f_{al}^{O2} + f_{al}^{O3} + f_a^{O}\right)/2 + 2f_{COO} + f_{CO} \le R_{O/C} \le f_{al}^{O2} + f_{al}^{O3} + f_a^{O} + 2f_{COO} + f_{CO}$

The substitute degree of aromatic rings (σ) not only reflects the structural characteristics of kerogen, but also has a clear relationship with the thermal maturity as the σ value decreases with increasing aromaticity [8]. Similarly to other kerogens at low thermal maturity level, Huadian oil shale kerogen has a high substitute degree of aromatic rings. The σ value of 0.51 indicates that about half the aromatic carbon atoms are substituted, suggesting that the three-dimensional network of kerogen is highly crosslinked.

The average aliphatic carbon chain length (Cn) was calculated using the

Table 4. Structural parameters of Huadian oil shale kerogen derived from DP and CP ^{13}C NMR

Method (contact time)	f_a, %	f_{al}, %	*Cn*	σ	*C*	$R_{H/C}$	$R_{O/C}$
DP	20.23	77.37	7.5–12.1	0.51	8.50	1.572	0.086–0.131
CP (2 ms)	14.81	83.51	12.1–31.2	0.47	8.74	1.707	0.058–0.085
CP (1 ms)	12.32	85.54	13.1–39.2	0.53	9.23	1.724	0.065–0.095
CP (0.5 ms)	9.95	88.32	14.2–24.8	0.63	9.19	1.737	0.069–0.108
Model	20.13	77.15	7.36	0.54	8.0	1.572	0.101

total amount of aliphatic carbons. Accordingly, its definition is not limited to the length of the straight carbon chain. It is not feasible to determine the value of *Cn* due to the uncertainty of the type of the oxygen attached to the oxy-aromatic carbon. Nevertheless, assuming that all or none of these oxygen atoms are bonded to aliphatic carbon chains on the other side, the lower and upper limits of *Cn* can be obtained. As seen from Table 3, *Cn* indicates the length of side chains of about 10 carbon atoms on average and that of bridges between two different aromatic clusters of about 20 carbon atoms. The length of bridges should be much greater than that of side chains because kerogen has a highly crosslinked molecular structure. Therefore, the aliphatic chains contain slightly less than 20 carbon atoms on average. This is consistent with the results of fast pyrolysis experiments, which show that at 600–700 °C, most alkanes and alkenes in the shale oil products contain around 20 carbon atoms [40]. The *Cn* values reported in previous studies on Huadian oil shale kerogen [16, 19, 37, 38] were higher than the *Cn* value obtained in the current research because CP underestimated the aromaticity and the average chain length was defined differently.

The average number of carbons per aromatic cluster (*C*) was defined on the assumption that the aromatic cluster size does not exceed two rings. Since Huadian oil shale kerogen mainly possesses aromatic clusters of 1–2 rings referring to the fast pyrolysis studies [40, 42], the *C* value calculated by the equation given in Table 3 is accurate enough. The *C* value of 8.5 indicates that there are slightly more naphthalene units in this kerogen than benzene units.

The definition of H/C atomic ratio ($R_{H/C}$) derived from ^{13}C NMR is presented in Table 3. For this definition, we assumed that all –COO groups were present in the form of carboxyl (–COOH) and that other hydrogen-containing groups such as hydroxyl and amino could be ignored. As the content of all these groups in Huadian oil shale kerogen is low [16] and these two assumptions

have competing effects on the H/C atomic ratio, $R_{H/C}$ can effectively provide a semiquantitative result of the H/C atomic ratio. The $R_{H/C}$ value given by DP (see Table 4) is in excellent agreement with the ultimate analysis result.

Oxygen-containing functional groups play an important role in the chemical stability of kerogen structure and the connection between kerogen and other components of oil shale [38, 43]. The organic oxygen content can be roughly estimated by the fractions of oxy-carbons, although the exact amount of organic oxygen cannot be obtained due to the unknown content of etheric carbon and hydroxyl [5, 8]. Given that the carbon atoms bound to oxygen by single bonds (f_{al}^{02}, f_{al}^{02}, f_{al}^{02}) are all present in ethers or are all attached to hydroxyls (as discussed in Section 3.1, no O–C–O exists in Huadian kerogen), the range of $R_{O/C}$ is defined (see Table 3). The DP-derived $R_{O/C}$ value (see Table 4) is consistent with the ultimate analysis result.

3.4. Quantitative reliability of DP/MAS spectrum

Experimental parameters, such as recycle delay and spinning frequency, have an important effect on the quantification of DP/MAS experiments. These parameters need to be set carefully to ensure the quantitative reliability of the DP spectrum.

3.4.1. Recycle delay

To gain the quantification for the DP spectrum, the recycle delay must be ca five times as long as the longest ^{13}C spin-lattice relaxation time ($T_{1,C}$) of the sample. In solid samples, the longest $T_{1,C}$ can be as long as tens of seconds or even longer [44]. This implies that DP measurements require extremely long experimental time to achieve favorable signal to noise ratios. However, Huadian oil shale kerogen is a low maturity kerogen with high H/C and O/C atomic ratios, which indicates that there are more protons and paramagnetic oxygen near the ^{13}C nuclei of each carbon type in this kerogen [44]. Consequently, the ^{13}C relaxation rates are accelerated by the strong dipole-dipole interaction. In this case, the longest $T_{1,C}$ is generally within 10 s [31, 45]. Correspondingly, the recycle delay of 50 s for the DP spectrum is sufficiently long for quantitative purposes.

3.4.2. MAS frequency

If the magic angle spinning frequency is small compared with the chemical shift anisotropy, spinning sidebands can be observed in the spectra, which reduce the centerband intensities and overlap with other signals. Previous ^{13}C NMR experiments performed in a 400 MHz spectrometer often used a MAS frequency of 5 kHz [16, 19, 37]. Since the MAS frequency is not high enough compared with the CSAs of the two types of ^{13}C nuclei, the intensities

of both the aromatic and aliphatic centerbands are weakened. Moreover, the band intensities of the oxy-carbon at 80 ppm and 180 ppm will be increased because of the overlap of the sidebands. Since the oxy-carbon intensities are usually low, the bands at these two chemical shifts will show a certain degree of symmetry if the aromatic sidebands are of relatively high intensity [16]. The aliphatic oxy-carbon band at 80 ppm is likely to be more severely affected as long as both the aliphatic and aromatic sidebands have a considerable intensity [37]. As a result, the intensities of oxy-carbon bands relative to the aromatic band are overestimated.

In the present study, a spinning frequency of 10 kHz is applied to remove the influence of sidebands. Since the spinning frequency is much greater than the CSAs of aliphatic ^{13}C nuclei, which are within 50 ppm [46] in our case, the intensity of aliphatic sidebands is negligible. For the aromatic centerband at 130 ppm, the most aromatic ^{13}C nuclei have a CSA value of about 100 ppm [46], which is comparable to the spinning frequency value. Hence, the aromatic sidebands can be reduced to an acceptable intensity [23]. Additionally, corresponding to the spinning frequency of 10 kHz and the ^{13}C Larmor frequency of 100 MHz, an aromatic sideband should be at 30 ppm (the others at multiples of 100 ppm from the centerband can be ignored because of their low intensities or no overlap with the regular signals) where the methylene band is extremely strong and largely unaffected. There is no observable sideband at –70 ppm and 230 ppm, which also suggests that the sidebands are substantially removed. The MAS frequency of 10 kHz should be considered as the minimum value for obtaining a quantitative DP/MAS spectrum of low aromaticity kerogens. For kerogen of higher aromaticity, a MAS frequency of 14 kHz or higher is more suitable [31].

3.5. Comparison of CP and DP spectra

As shown in Figure 1, the aliphatic signals in the CP spectra are much stronger compared with the DP spectrum. For the quantification process of the CP spectra the same methods were used as for the DP spectrum. The deduced structural parameters are listed in Table 4. The distribution and widths of the simulated peaks for the CP spectra are similar to those of the DP spectrum (Fig. 2), which ensures that the structural parameters derived from these two techniques are comparable.

Consistent with the intensities of the main peaks in each spectrum, the CP spectra provide evidently higher values of aliphaticity (f_{al}), Cn and $R_{H/C}$ than the DP spectrum, depicting kerogen structures with more and longer aliphatic carbon chains. On the other hand, all the f_a values obtained from the CP spectra are much lower than the f_a value from the DP spectrum. These findings indicate that the CP/MAS experiments underestimate the amount of aromatic carbons because of the insufficient polarization transfer from ^{1}H spins to aromatic ^{13}C spins.

Although the CP-derived aromaticity increases from 9.95% to 14.81% as

the contact time increases from 0.5 ms to 2 ms, an accurate aromaticity cannot be obtained by further increasing the contact time. With contact times shorter than 2 ms, the polarization transfer from ^{1}H spins to aromatic ^{13}C spins is quite insignificant, which arises from the long polarization-transfer time (T_{CH}) of aromatic ^{13}C nuclei. Consequently, the aromatic carbon intensity benefits more from the increasing contact time. However, experiments using variable contact times show that both the aliphatic and aromatic signals decrease due to the proton rotating-frame spin-lattice relaxation effect [23, 29]. Especially with a contact time exceeding 2 ms, the relative intensities of these signals tend to remain constant [47]. In fact, the long T_{CH} of aromatic ^{13}C nuclei is not the main reason for the loss of the aromatic signal in CP [23]. This is especially true for the present sample, in which the aromatic T_{CH} is relatively short due to the small aromatic cluster size. On the other hand, the paramagnetic centers such as organic radicals, paramagnetic oxygen and Fe [16] in the low-maturity kerogen under study are of high content and are mainly located in the aromatic regions, which greatly shortens the aromatic proton rotating-frame spin-lattice relaxation time ($T_{1\rho,H}$) and reduces the polarization transfer to the aromatic carbon [23, 44]. As a consequence, a portion of the aromatic carbon content is undetectable in CP, which means that CP underestimates the aromaticity regardless of the contact time. The paramagnetic centers have a minor influence on the DP experiment because usually more than 80% of the potential ^{13}C signals can be detected in these experiments with low-maturity samples, indicating the quantitative reliability of this technique [27].

Moreover, the σ values from the CP spectra show a significant uncertainty due to their high dependence on the contact times used in CP. All the *C* values determined from the CP spectra are slightly higher than the *C* value derived from the DP spectrum, which indicates that a much smaller number of aromatic clusters in the kerogen model of a certain size will be obtained from the CP spectra, given that the f_a value is lower. The results of $R_{O/C}$ show that the amount of organic oxygen is underestimated by CP, probably because part of the oxy-carbon is not sufficiently polarized in CP. The underestimated organic oxygen content suggests fewer reaction sites in the kerogen structure derived from CP spectra.

There is a close relationship between the H/C atomic ratio and aromaticity. A higher aromaticity usually means a lower H/C atomic ratio and vice versa. The $R_{H/C}$ derived from DP is very close to that from the ultimate analysis, which suggests the accuracy of DP aromaticity. At the same time, all the CP spectra give a much higher $R_{H/C}$ value than ultimate analysis, which may be explained by the underestimation of aromaticity by the former. A previous modeling study of Huadian oil shale kerogen by Tong et al. [20] shows the effect of the contradiction between the aromaticity from ^{13}C NMR and the H/C atomic ratio from ultimate analysis. The kerogen models are based on the ^{13}C CP/MAS NMR spectrum with a 5-kHz spinning frequency, which gives a much lower aromaticity (f_a = 9.7%) than the DP/MAS spectrum [16], and even lower than the CP/MAS spectra in the current study due to the low MAS

frequency. In this case, the aromaticity and H/C atomic ratio of the models cannot match the experimental data simultaneously. As a consequence, the models are a compromise between these two parameters and cannot accurately reflect the kerogen structure.

Furthermore, if the CP-derived kerogen models are used in its simulation studies, the behavior of the models will be severely affected by the inaccurate aromaticity and H/C atomic ratio because these parameters determine the overall characteristics of the molecular models [22]. This will lead to the misunderstanding of the reaction mechanism of the kerogen pyrolysis and combustion. Therefore, DP/MAS at a high spinning frequency is necessary for the characterization of kerogen, especially when the results are used as a data source for its modeling.

3.6. Approximate molecular model

Based on the DP NMR results, an approximate molecular model of kerogen (Fig. 3) was built to present its structural features and validate the consistency of the respective data. The chemical formula of the model is $C_{477}H_{750}O_{48}$ and the molecular mass is 7248. Most of the functional group fractions and the structural parameters of the model (see Table 2 and Table 4) are well matched with the experimental results, indicating the accuracy of the model and the rationality of the spectral fitting.

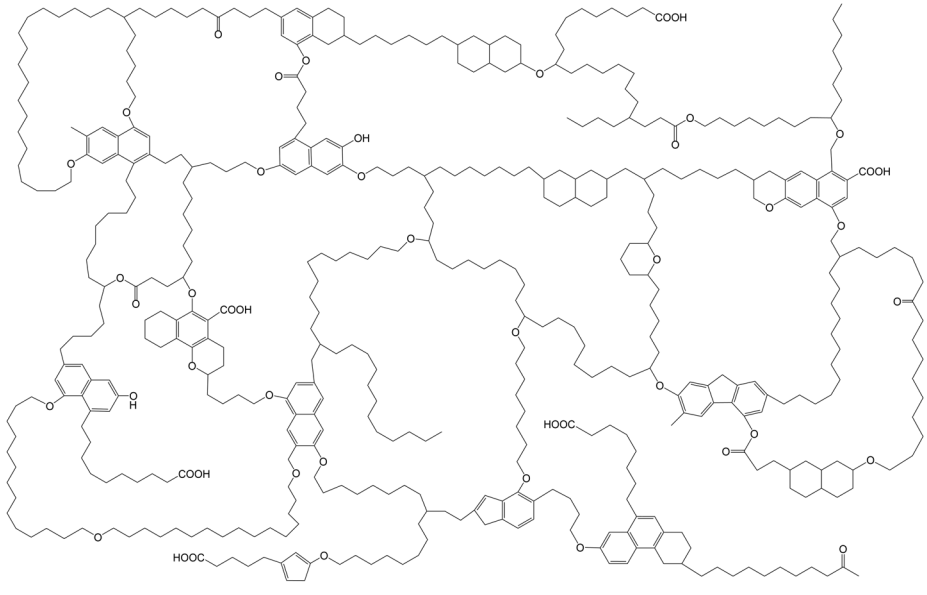

Fig. 3. An approximate molecular model of Huadian oil shale kerogen. The chemical formula is $C_{477}H_{750}O_{48}$.

4. Conclusions

In this study, direct polarization and cross polarization ^{13}C solid-state nuclear magnetic resonance spectra were obtained and spinning sidebands were avoided by applying a high magic angle spinning frequency of 10 kHz. The quantitative DP results show that the Huadian oil shale kerogen is highly aliphatic and its aromaticity is low, 20.23%. Consistent with this, the kerogen has a great average aliphatic carbon chain length ($Cn \approx 10$) and a small average aromatic cluster size ($C = 8.5$). The substitute degree of aromatic rings is as high as 0.51, suggesting that the three-dimensional network of the kerogen is highly crosslinked. The H/C and O/C atomic ratios derived from DP are in agreement with ultimate analysis results, which suggests the quantitative reliability of this technique.

All ^{13}C CP/MAS NMR spectra greatly underestimate the aromaticity of the kerogen. The other structural parameters given by CP are also evidently different from the corresponding results from DP. The CP-derived H/C atomic ratios are much higher than the respective ratio from ultimate analysis, which gives evidence of the unsuitability of CP for a quantitative characterization of kerogen. It is concluded that when quantitative structural information on kerogen is needed, especially for molecular modeling, DP and a high MAS frequency are necessary.

Acknowledgements

This work was supported by the National Natural Science Foundation of China (Grant Nos. 51876122, 21673148).

REFERENCES

1. Tissot, B. P., Welte, D. H. *Petroleum Formation and Occurrence*. Springer-Verlag, New York, 1984.
2. Han, X. X., Kulaots, I., Jiang, X. M., Suuberg, E. M. Review of oil shale semicoke and its combustion utilization. *Fuel*, 2014, **126**, 143–161.
3. Oh, M. S., Taylor, R. W., Coburn, T. T., Crawford, R. W. Ammonia evolution during oil shale pyrolysis. *Energy Fuels*, 1988, **2**(1), 100–105.
4. Behar, F., Vandenbroucke, M. Chemical modelling of kerogens. *Org. Geochem.*, 1987, **11**(1), 15–24.
5. Trewhella, M. J., Poplett, I.J. F., Grint, A. Structure of Green River oil shale kerogen: Determination using solid state ^{13}C n.m.r. spectroscopy. *Fuel*, 1986, **65**(4), 541–546.
6. Kister, J., Guiliano, M., Largeau, C., Derenne, S., Casadevall, E. Characterization of chemical structure, degree of maturation and oil potential of Torbanites (type I

kerogens) by quantitative FT-i.r. spectroscopy. *Fuel*, 1990, **69**(11), 1356–1361.
7. Kelemen, S. R., Freund, H., Gorbaty, M. L., Kwiatek, P. J. Thermal chemistry of nitrogen in kerogen and low-rank coal. *Energy Fuels*, 1999, **13**(2), 529–538.
8. Kelemen, S. R., Afeworki, M., Gorbaty, M. L., Sansone, M., Kwiatek, P. J., Walters, C. C., Freund, H., Siskin, M., Bence, A. E., Curry, D. J., Solum, M., Pugmire, R. J., Vandenbroucke, M., Leblond, M., Behar, F. Direct characterization of kerogen by X-ray and solid-state ^{13}C nuclear magnetic resonance methods. *Energy Fuels*, 2007, **21**(3), 1548–1561.
9. Fletcher, T. H., Gillis, R., Adams, J., Hall, T., Mayne, C. L., Solum, M. S., Pugmire, R. J. Characterization of macromolecular structure elements from a Green River oil shale, II. Characterization of pyrolysis products by ^{13}C NMR, GC/MS, and FTIR. *Energy Fuels*, 2014, **28**(5), 2959–2970.
10. Wang, Q., Hou, Y. C., Wu, W. Z., Yu, Z., Ren, S. H., Liu, Q. Y., Liu, Z. Y. A study on the structure of Yilan oil shale kerogen based on its alkali-oxygen oxidation yields of benzene carboxylic acids, ^{13}C NMR and XPS. *Fuel Process. Technol.*, 2017, **166**, 30–40.
11. Chu, W. Y., Cao, X. Y., Schmidt-Rohr, K., Birdwell, J. E., Mao, J. D. Investigation into the effect of heteroatom content on kerogen structure using advanced ^{13}C solid-state nuclear magnetic resonance spectroscopy. *Energy Fuels*, 2019, **33**(2), 645–653.
12. Cao, X. Y., Yang, J., Mao, J. D. Characterization of kerogen using solid-state nuclear magnetic resonance spectroscopy: A review. *Int. J. Coal Geol.*, 2013, **108**, 83–90.
13. Pines, A., Gibby, M. G., Waugh, J. S. Proton-enhanced NMR of dilute spins in solids. *J. Chem. Phys.*, 1973, **59**(2), 569–590.
14. Mann, A. I., Patience, R. I., Poplett, I. J. F. Determination of molecular structure of kerogens using ^{13}C NMR spectroscopy: I. The effects of variation in kerogen type. *Geochim. Cosmochim. Acta*, 1991, **55**(8), 2259–2268.
15. Lille, Ü., Heinmaa, I., Müürisepp, A. M., Pehk, T. Investigation of kukersite structure using NMR and oxidative cleavage: On the nature of phenolic precursors in the kerogen of Estonian kukersite. *Oil Shale*, 2002, **19**(2), 101–116.
16. Tong, J. H., Han, X. X., Wang, S., Jiang, X. M. Evaluation of structural characteristics of Huadian oil shale kerogen using direct techniques (solid-state ^{13}C NMR, XPS, FT-IR, and XRD). *Energy Fuels*, 2011, **25**(9), 4006–4013.
17. Orendt, A. M., Pimienta, I. S. O., Badu, S. R., Solum, M. S., Pugmire, R. J., Facelli, J. C., Locke, D. R., Chapman, K. W., Chupas, P. J., Winans, R. E. Three-dimensional structure of the Siskin Green River oil shale kerogen model: A comparison between calculated and observed properties. *Energy Fuels*, 2013, **27**(2), 702–710.
18. Ungerer, P., Collell, J., Yiannourakou, M. Molecular modeling of the volumetric and thermodynamic properties of kerogen: Influence of organic type and maturity. *Energy Fuels*, 2015, **29**(1), 91–105.
19. Guan, X. H., Liu, Y., Wang, D., Wang, Q., Chi, M. S., Liu, S., Liu, C. G. Three-dimensional structure of a Huadian oil shale kerogen model: An experimental

and theoretical study. *Energy Fuels*, 2015, **29**(7), 4122-4136.

20. Tong, J. H., Jiang, X. M., Han, X. X., Wang, X. Y. Evaluation of the macromolecular structure of Huadian oil shale kerogen using molecular modeling. *Fuel*, 2016, **181**, 330–339.
21. Katti, D. R., Thapa, K. B., Katti, K. S. Modeling molecular interactions of sodium montmorillonite clay with 3D kerogen models. *Fuel*, 2017, **199**, 641–652.
22. Rogel, E. Simulation of interactions in asphaltene aggregates. *Energy Fuels*, 2000, **14**(3), 566–574.
23. Wind, R. A., Maciel, G. E., Botto, R. E. Quantitation in ^{13}C NMR spectroscopy of carbonaceous solids. In: *Magnetic Resonance of Carbonaceous Solids* (Botto, R. E., Sanada, Y., eds.), Advances in Chemistry, **229**. American Chemical Society, Washington, DC, 1992, 3–26.
24. Miknis, F. P. Applications of solid-state NMR in oil shale research. In: *Annual Reports on NMR Spectroscopy*, **33**. Academic Press, 1996, 207–246.
25. Smernik, R. J., Oades, J. M. The use of spin counting for determining quantitation in solid state ^{13}C NMR spectra of natural organic matter 1. Model systems and the effects of paramagnetic impurities. *Geoderma*, 2000, **96**(1–2), 101–129.
26. Snape, C. E., Axelson, D. E., Botto, R. E., Delpuech, J. J., Tekely, P., Gerstein, B. C., Pruski, M., Maciel, G. E., Wilson, M. A. Quantitative reliability of aromaticity and related measurements on coals by ^{13}C n.m.r. A debate. *Fuel*, 1989, **68**(5), 547–548.
27. Smernik, R. J., Schwark, L., Schmidt, M. W. I. Assessing the quantitative reliability of solid-state ^{13}C NMR spectra of kerogens across a gradient of thermal maturity. *Solid State Nucl. Magn. Reson.*, 2006, **29**(4), 312–321.
28. Mao, J. D., Cao, X. Y., Olk, D. C., Chu, W. Y., Schmidt-Rohr, K. Advanced solid-state NMR spectroscopy of natural organic matter. *Prog. Nucl. Magn. Reson. Spectrosc.*, 2017, **100**, 17–51.
29. Botto, R. E., Wilson, R., Winans, R. E. Evaluation of the reliability of solid ^{13}C-NMR spectroscopy for the quantitative analysis of coals: Study of whole coals and maceral concentrates. *Energy Fuels*, 1987, **1**(2), 173–181.
30. Fang, X. W., Chua, T., Schmidt-Rohr, K., Thompson, M. L. Quantitative ^{13}C NMR of whole and fractionated Iowa Mollisols for assessment of organic matter composition. *Geochim. Cosmochim. Acta*, 2010, **74**(2), 584–598.
31. Mao, J. D., Fang, X. W., Lan, Y. Q., Schimmelmann, A., Mastalerz, M., Xu, L., Schmidt-Rohr, K. Chemical and nanometer-scale structure of kerogen and its change during thermal maturation investigated by advanced solid-state ^{13}C NMR spectroscopy. *Geochim. Cosmochim. Acta*, 2010, **74**(7), 2110–2127.
32. Gao, Y., Zou, Y. R., Liang, T., Peng, P. A. Jump in the structure of Type I kerogen revealed from pyrolysis and ^{13}C DP MAS NMR. *Org. Geochem.*, 2017, **112**, 105–118.
33. Maroto-Valer, M. M., Taulbee, D. N., Andrésen, J. M., Hower, J. C., Snape, C. E. Quantitative ^{13}C NMR study of structural variations within the vitrinite and inertinite maceral groups for a semifusinite-rich bituminous coal. *Fuel*, 1998, **77**(8), 805–813.

34. Mao, J. D., Hu, W. G., Schmidt-Rohr, K., Davies, G., Ghabbour, E. A., Xing, B. Quantitative characterization of humic substances by solid-state carbon-13 nuclear magnetic resonance. *Soil Sci. Soc. Am. J.*, 2000, **64**(3), 873–884.
35. Durand, B., Nicaise, G. Procedures for kerogen isolation. In: *Kerogen-Insoluble Organic Matter from Sedimentary Rocks* (Durand, B., ed.). Editions Technip, Paris, 1980, 35–53.
36. Massiot, D., Fayon, F., Capron, M., King, I., Le Calvé, S., Alonso, B., Durand, J.-O., Bujoli, B., Gan, Z., Hoatson, G. Modelling one- and two-dimensional solid-state NMR spectra. *Magn. Reson. Chem.*, 2002, **40**(1), 70–76.
37. You, Y. L., Han, X. X., Liu, J. G., Jiang, X. M. Structural characteristics and pyrolysis behaviors of Huadian oil shale kerogens using solid-state ^{13}C NMR, Py-GCMS and TG. *J. Therm. Anal. Calorim.*, 2018, **131**(2), 1845–1855.
38. Ru, X., Cheng, Z., Song, L., Wang, H., Li, J. Experimental and computational studies on the average molecular structure of Chinese Huadian oil shale kerogen. *J. Mol. Struct.*, 2012, **1030**, 10–18.
39. Siskin, M., Scouten, C. G., Rose, K. D., Aczel, T., Colgrove, S. G., Pabst Jr., R. E. Detailed structural characterization of the organic material in Rundle Ramsay Crossing and Green River oil shales. In: *Composition, Geochemistry and Conversion of Oil Shales* (Snape, C., ed.), NATO ASI Series, 455, Springer Netherlands, 1995, 143–158.
40. Huang, Y. R., Han, X. X., Jiang, X. M. Characterization of Dachengzi oil shale fast pyrolysis by Curie-point pyrolysis-GC-MS. *Oil Shale*, 2015, **32**(2), 134–150.
41. Solum, M. S., Pugmire, R. J., Grant, D. M. Carbon-13 solid-state NMR of Argonne-premium coals. *Energy Fuels*, 1989, **3**(2), 187–193.
42. Huang, Y. R., Han, X. X., Jiang, X. M. Comparison of fast pyrolysis characteristics of Huadian oil shales from different mines using Curie-point pyrolysis-GC/MS. *Fuel Process. Technol.*, 2014, **128**, 456–460.
43. Razvigorova, M., Budinova, T., Tsyntsarski, B., Petrova, B., Ekinci, E., Atakul, H. The composition of acids in bitumen and in products from saponification of kerogen: Investigation of their role as connecting kerogen and mineral matrix. *Int. J. Coal Geol.*, 2008, **76**(3), 243–249.
44. Wind, R. A., Duijvestijn, M. J., van der Lugt, C., Smidt, J., Vriend, H. An investigation of coal by means of e.s.r., ^{1}H n.m.r., ^{13}C n.m.r. and dynamic nuclear polarization. *Fuel*, 1987, **66**(7), 876–885.
45. Cao, X. Y., Birdwell, J. E., Chappell, M. A., Li, Y., Pignatello, J. J., Mao, J. D. Characterization of oil shale, isolated kerogen, and post-pyrolysis residues using advanced ^{13}C solid-state nuclear magnetic resonance spectroscopy. *AAPG Bull.*, 2013, **97**(3), 421–436.
46. Veeman, W. S. Carbon-13 chemical shift anisotropy. *Prog. Nucl. Magn. Reson. Spectrosc.*, 1984, **16**, 193–235.
47. Snape, C. E., McGhee, B. J., Martin, S. C., Andresen, J. M. Structural characterisation of catalytic coke by solid-state ^{13}C-NMR spectroscopy. *Catal. Today*, 1997, **37**(3), 285–293.